ISSN 1070-4272, Russian Journal of Applied Chemistry, 2016, Vol. 89, No. 9, pp. 1402−1408. © Pleiades Publishing, Ltd., 2016.
Original Russian Text © A.S. Kondrateva, S.E. Alexandrov, 2016, published in Zhurnal Prikladnoi Khimii, 2016, Vol. 89, No. 9, pp. 1108−1114.

INORGANIC SYNTHESIS AND INDUSTRIAL INORGANIC CHEMISTRY

Fundamental Physicochemical Regularities of the Chemical Vapor Deposition of Nickel Oxide Layers

A. S. Kondrateva* and S. E. Alexandrov

Peter the Great St. Petersburg Polytechnic University, ul. Politekhnicheskaya 29/1, St. Petersburg, 195251 Russia
** e-mail: a_kondrateva@spbstu.ru*

Received June 28, 2016

Abstract—Physicochemical regularities of the chemical vapor deposition (CVD) of nickel oxide layers in the $(EtCp)_2Ni–O_3–O_2–Ar$ reaction system at a reduced pressure were studied. Dependences of growth rate of NiO layers on deposition temperature, linear gas flow velocity, and roughness were derived. A mass-spectrometric study of the composition of the reaction gas phases formed in these systems provided evidence about the fundamental physicochemical regularities of the CVD process, which is important for solving applied problems associated with the development of technological equipment and industrial technology for deposition of NiO layers.

DOI: 10.1134/S1070427216090032

Nickel oxide (NiO) layers exhibit a unique set of properties, which gives reason to believe that these layers can be used as oxide material in resistive switches, magnetic material in nonvolatile information-storage devices, material of electrodes for electrochemical cells for different devices, sensitive of gas sensors, catalyst for decomposition of organic substances, etc. [1–4].

There are a lot of physical and chemical methods for obtaining NiO layers [5–9]. One of modern chemical deposition methods used for this purpose is the chemical vapor deposition (CVD). This technique enables reliable control over the composition and structure of the product being formed and reproducible deposition of thickness-uniform layers with good adhesion. Despite that, only a small number of publications have been devoted to CVD of NiO layers. Research teams have suggested nickel carbonyl $Ni(CO)_4$, nickel acetylacetonate $Ni(C_5H_7O_2)_2 \times H_2O$, nickelocene $Ni(Cp)_2$, and its homologs as CVD precursors [6, 10–15]. It has been shown that, even with oxygen-containing starting reagents, such as nickel β-diketonates and β-dioxymates, it is necessary to additionally introduce oxygen to obtain oxide layers of stoichiometric composition [4]. Deposition of NiO at low temperatures is topical for extending the variety of substrate materials. It s known [13] that introduction of ozone into the reaction system can occasionally diminish the deposition onset temperature. The use of ozone as oxidizing agent for CVD in deposition of NiO layers from $(EtCp)_2Ni$ has not been studied previously.

The goal of our study was to examine the fundamental physicochemical aspects of the CVD of NiO layers in the $(EtCp)_2Ni–O_3–O_2–Ar$ reaction system, find the rate-determining stage under the technological conditions under study, and compare the process with the deposition in the $(EtCp)_2Ni–O_2–Ar$ system.

EXPERIMENTAL

NiO layers were deposited in an experimental CVD reactor at a reduced pressure with independent reactants lines [16]. The process was performed in a horizontal quartz reactor with “hot walls.” Experiments were performed with polished silicon wafers (100), (*n*-Si : P with resistivity of 4.5 Ω cm), (111), and (100) (*p*-Si : B with resistivity of 7.5 Ω cm). For some experiments, the surface area of the substrates was changed by electrochemical etching. The technological deposition zone was situated at the beginning of the isothermal zone of the reactor furnace. Within the chosen region, the thickness-nonuniformity of the layers did not exceed

5%. Argon was used as diluent gas and carrier gas for $(EtCp)_2Ni$. The experiments were performed under the following conditions: total flow rate of the working mixture Q = 200 mL min^{-1}, total pressure P = 500–1500 Pa, deposition temperature T = 620–770 K, molar flow rate $q[(EtCp)_2Ni]$ = 1.8–4.7 μmol min^{-1}. oxygen flow rate $Q(O_2)$ = 40 mL min^{-1}, ozone partial pressure $P(O_3)$ = 0–60 Pa, and deposition duration τ = 5–90 min.

The thickness of the layers was determined by measuring the fluorescence intensity of the characteristic nickel line (at a wavelength of 0.166 nm, which corresponds to the photon energy of electromagnetic radiation of 7.47 eV) in an X-ray fluorescence analysis on a Spectroscan MAKS-GV spectrometer. The calibration was made by measuring the layer thickness on cleaved substrates with a Carl Zeiss 55 Supra 55VP with an accuracy of ±4 nm. A SolverPRO NT-MDT atomic-force microscope was used to determine the actual surface area of the substrates and the morphology of the layers. An X-ray phase analysis was made with a Super Nova Dual Wavelength diffractometer (Agilent Technologies) (CuK_α radiation, λ = 1.5405 Å). The chemical composition was analyzed by X-ray photoelectron spectroscopy (XPS) with a Thermo Scientific K-α complex. A mass-spectrometric analysis of the reaction gas phase was carried out with an MCX-6 time-of-flight mass spectrometer with the energy of the ionizing beam of 100 eV. The mass spectra were normalized to the amplitude of the peak with m/z = 20 Da, associated with the Ar^{2+} ion.

RESULTS AND DISCUSSION

Preliminary experiments demonstrated that the time dependences of the thickness of the NiO layers were linear within experimental inaccuracy (Fig. 1, curves *1–3*) for temperatures of 670–and 720 K. For this reason, the numerical value of the deposition rate can be calculated as the ratio between the thickness of a layer and the process duration.

The average deposition rate in the $(EtCp)_2Ni–O_3–O_2–Ar$ system at 670 K (Fig. 1, curve *1*) was 120 nm h^{-1}, and that at 720 K (curve *2*), 380 nm h^{-1}. For the $(EtCp)_2Ni–O_2–Ar$ system at 670 K (curve *3*), it was 260 nm h^{-1}. Thus, the introduction of ozone made lower the average growth rate of the layers.

The temperature dependences of the NiO layer deposition rate, plotted in the Arrhenius coordinates (Fig. 2), changed their slope at around 740 K. The run of the dependences remained the same for substrates with different crystallographic orientations and doping levels (Fig. 2, curves *1*). At temperature range 630–720 K, the apparent activation energy of the process was 83 ± 5 kJ mol^{-1}.

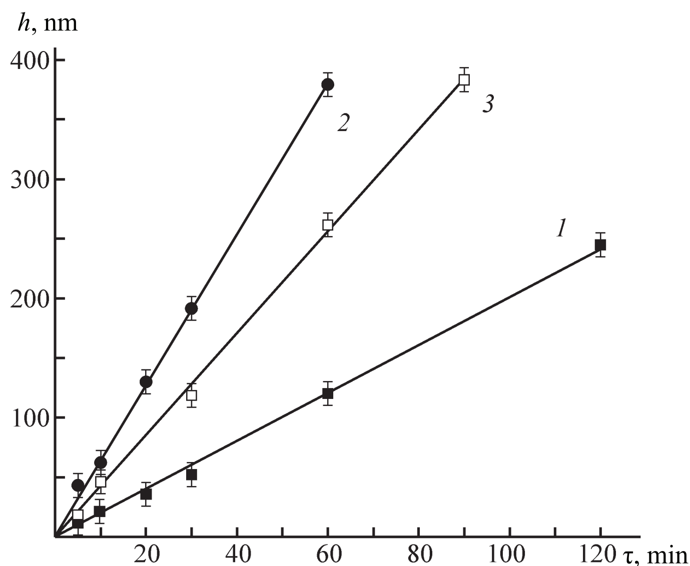

Fig. 1. Thickness h of NiO layers being deposited vs. the process duration τ. KEF-4.5 (100) substrates, P = 840 Pa, $q[(EtCp)_2Ni]$ = 2.7 μmol min^{-1}, $P(O_3)$ = 5 and 0 Pa, $Q(O_2)$ = 40 mL min^{-1}, Q = 200 mL min^{-1}, τ = 60 min, T = 640 K. (*1*) $(EtCp)_2Ni–O_3–O_2–Ar$, 670 K; (*2*) $(EtCp)_2Ni–O_3–O_2–Ar$, 720 K; (*3*) $(EtCp)_2Ni–O_2–Ar$, 670 K.

At temperatures above 740 K, the apparent activation energy decreased to 18 ± 7 kJ mol^{-1}, with even negative values observed at a low gas flow velocity in the reactor. In all probability, this effect is due to the depletion of the reaction mixture of the reagent as a result of its consumption for deposition of an oxide layer on the walls of the reaction chamber before the technological deposition zone, which was confirmed by visual inspection. This assumption is also confirmed by mass-spectrometric data, according to which the conversion of the reagent reached the maximum value (90%) at around 700 K. These results indicate that, in the high-temperature range, the deposition rate is limited by the delivery of the reagent into the reaction zone.

To find the type of the rate-determining stage in the low-temperature range, we examined how the deposition rate of NiO layers depends on the linear flow velocity in the isothermal zone at 640 K at an invariable overall flow rate of gases. The linear flow velocity was varied by changing the reaction zone diameter (quartz inserts were

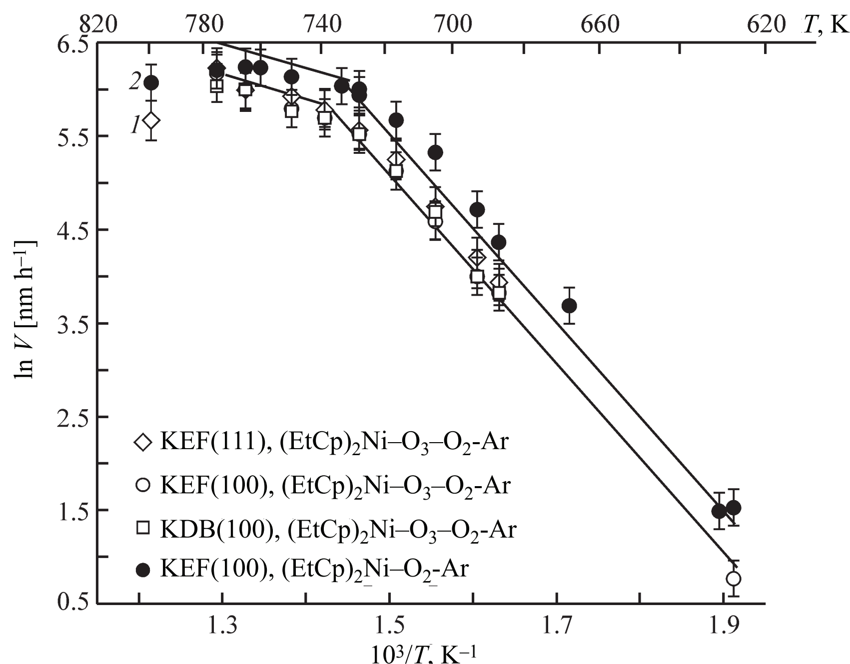

Fig. 2. Deposition rate V vs. temperature T in systems (*1*) $(EtCp)_2Ni–O_3–O_2–Ar$ and (*2*) $(EtCp)_2Ni–O_2–Ar$. P = 840 Pa, $q[(EtCp)_2Ni]$ = 2.7 μmol min^{-1}, $P(O_3)$ = 5 and 0 Pa, $Q(O_2)$ = 40 mL min^{-1}, Q = 200 mL min^{-1}, τ = 60 min.

used). The fact that the parameter under study has no effect on the rate (Table 1) may indicate that the process occurs under kinetic control.

We also examined how the deposition rate of NiO layers depends on the substrate surface area. The increase in the deposition rate, observed as the actual substrate area becomes larger due to the rise in roughness (Table 2), also shows that the process occurs under kinetic control.

The results obtained when studying the dependence of the deposition rate of NiO layers on the amount of reagents being delivered are presented in Fig. 3. It can be seen that the deposition rate linearly grows with increasing molar expenditure of $(EtCp)_2Ni$ (Fig. 3, curve *1*). The introduction of O_3 even in minor amounts (0–10 Pa) led to a significant decrease in the deposition rate (Fig. 3, curve *2*).

To determine the effect of ozone additive in more detail, we examined the composition of the reaction gas phase by TOF mass spectrometry. We employed the experimental procedure developed in the preceding studies of the CVD of nickel-based layers from $(EtCp)_2Ni$ [17].

Figure 4 shows typical mass spectra of the reaction gas phase formed in the $(EtCp)_2Ni–O_2–Ar$ and $(EtCp)_2Ni–O_3–O_2–Ar$ systems. The introduction of ozone gave rise to peaks with m/z 36, 58, 68, 100, 126, 193, and 291 Da,

Table 1. Layer deposition rate at various linear flow velocities KEF-4.5 (100) substrates, P = 840 Pa, $q[(EtCp)_2Ni]$ = 2.7 μmol min^{-1}, $P(O_3)$ = 5 Pa, $Q(O_2)$ = 40 mL min^{-1}, Q = 200 mL min^{-1}, τ = 60 min, T = 640 K

Linear flow velocity, m h^{-1}	Growth rate, nm h^{-1}
3.5	104 ± 5
4.6	97 ± 5
7.9	100 ± 5
15.8	95 ± 5

Table 2. Layer deposition rate at various roughnesses and substrate surface areas (20 mm²) KEF-4.5 (100) substrates, P = 840 Pa, $q[(EtCp)_2Ni]$ = 2.7 μmol min^{-1}, $P(O_3)$ = 5 Pa, $Q(O_2)$ = 40 mL min^{-1}, Q = 200 mL min^{-1}, τ = 60 min, T = 640 K

Arithmetic mean deviation of the surface profile, nm	Sample surface area, 10^{-7} m^2	Growth rate, nm h^{-1}
2	6	190 ± 5
113	395	295 ± 5
137	480	308 ± 5

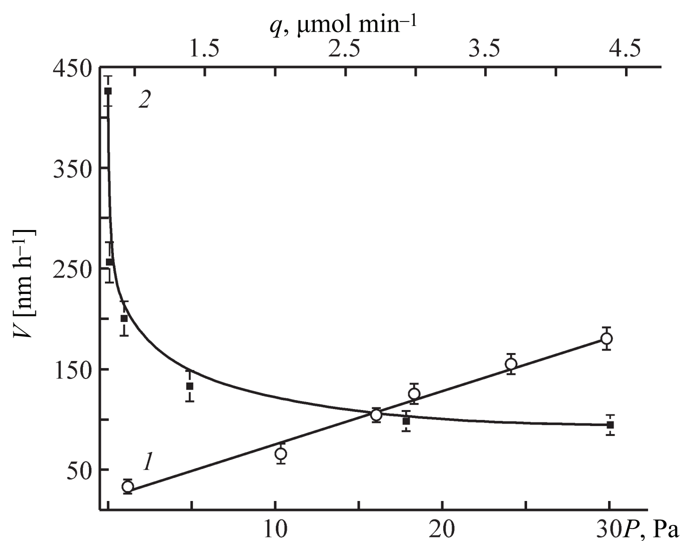

Fig. 3. Deposition rate V vs. the amount of the delivered reagents. KEF-4.5 (100) substrates, P = 840 Pa, q[$(EtCp)_2Ni$] = 2.7 μmol min^{-1} or $P(O_3)$ = 5 Pa, $Q(O_2)$ = 40 mL min^{-1}, Q = 200 mL min^{-1}, τ = 60 min.

not observed previously in mass spectra of the $(EtCp)_2Ni$–O_2–Ar system. These peaks are probably associated with products formed in the interaction of $(EtCp)_2Ni$ with ozone or with fragments of these. The intensity of the peak at 110 Da, associated with CpCOOH, decreased. Figure 5 shows temperature dependences of the peaks with *m/z* 110 and 80 Da in the absence and presence of ozone. Comparison of the intensities of the related peaks shows that the introduction of ozone made lower the CpCOOH formation probability of and had no effect on the CpO formation.

According to the available published evidence [18], ozonides are formed in the case of interaction of aromatic compounds with ozone in the gas phase and further undergo dissociation or stabilization. It has also been shown that no additional activation is necessary for aromatic compounds to interact with ozone at the double bond.

In view of this evidence, we can assume that the ozone molecule attacks the double bond of the cyclopentadienyl ring of the $(EtCp)_2Ni$ molecule to give an ozonide of the reagent, to which corresponds the peak with *m/z* 289 Da [Scheme 1, reaction (1)]. In the case of the dissociative pathway, the ozonide decomposes into a radical (nickel cyclopentadienyl) and ethyl pentenedial with *m/z* 126 Da [reaction (2)]. By analogy, ozone can attack the double bond of ethyl pentenedial to give ozonide [reaction (3)], which decomposes into ethyl propanedial (*m/z* 100 Da) and ethanedial (*m/z* 58 Da) [reaction (4)]. The suggested conversion scheme of $(EtCp)_2Ni$ is confirmed by the presence of the corresponding peaks in the mass spectra, which presumably indicates that ethanedial, ethyl propanedial, and ethy pentenedial are formed (Scheme 1).

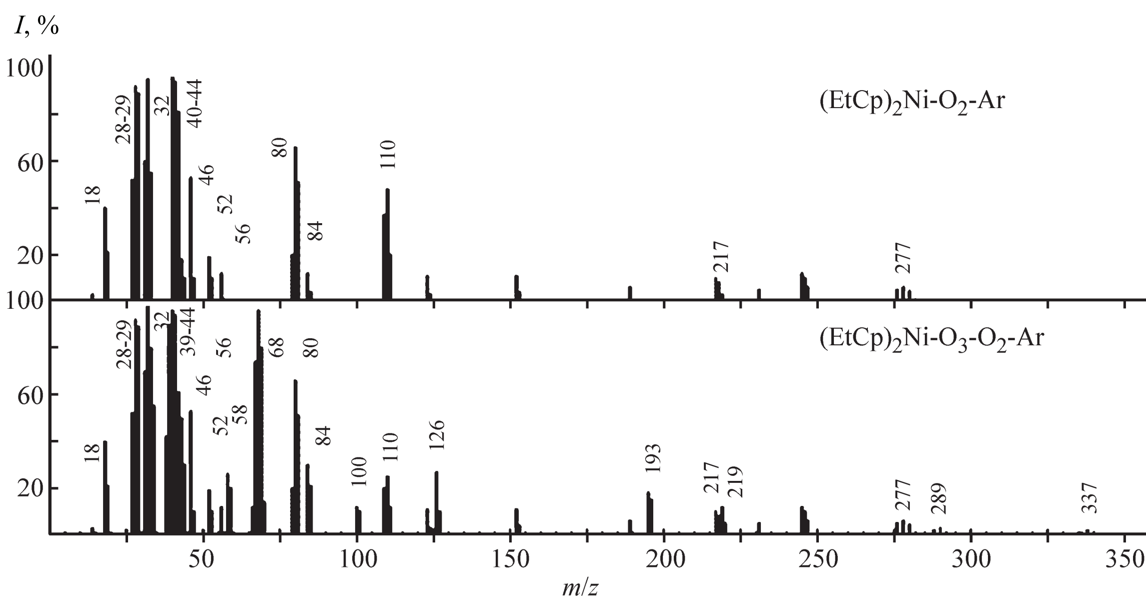

Fig. 4. Mass spectra of the gas phase from the deposition zone in the systems $(EtCp)_2Ni$–O_2–Ar and $(EtCp)_2Ni$–O_3–O_2–Ar at 480 K. (I) Intensity.

Scheme 1.

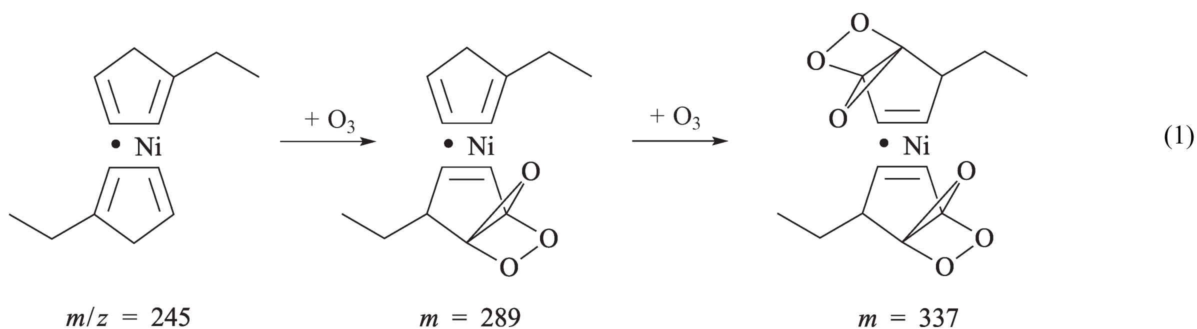

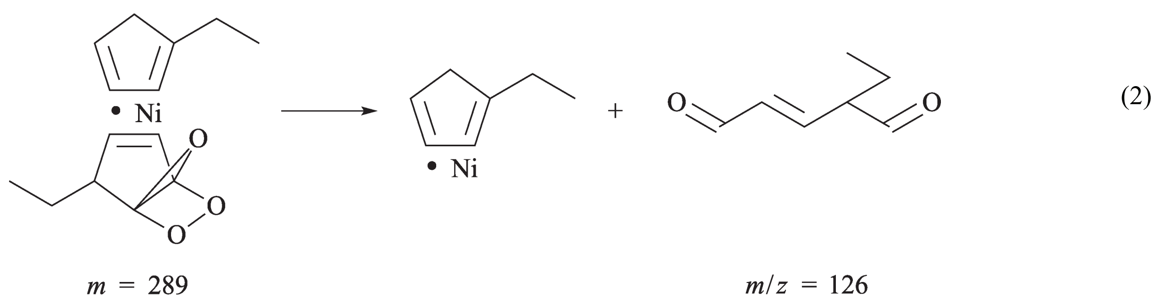

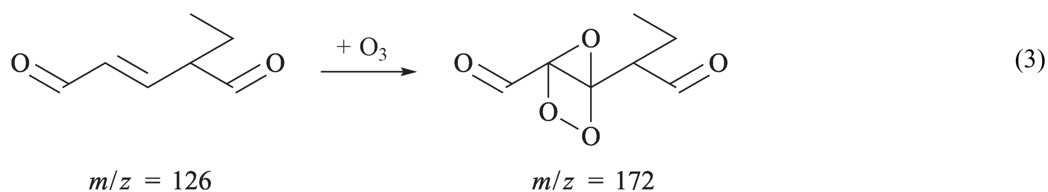

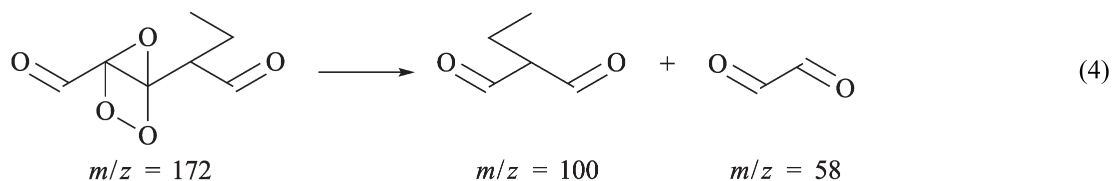

Scheme 2.

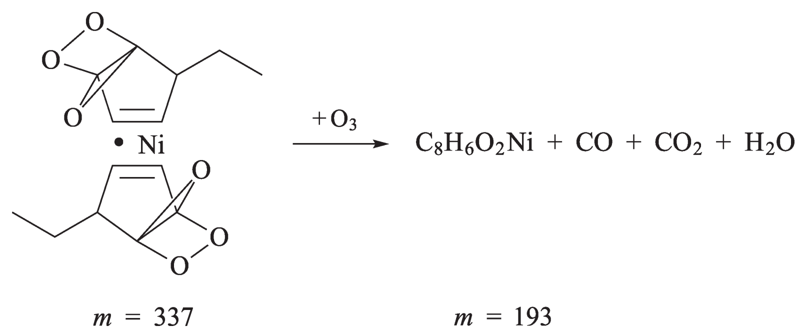

In the mass spectra, the intensities of the peaks corresponding to *m/z* 126, 100, and 58 Da (Fig. 6a) decrease with increasing temperature in the reaction zone. This indicates the decrease in the intensity of dialdehyde formation, which is, in all probability, due to the decrease in the concentration of ozone with increasing temperature as a result of its decomposition.

In the case of the stabilization pathway, ozonide of the reagent with *m/z* 337 Da is probably transformed to $C_8H_6O_2Ni$ (*m/z* 193 Da) (Scheme 2).

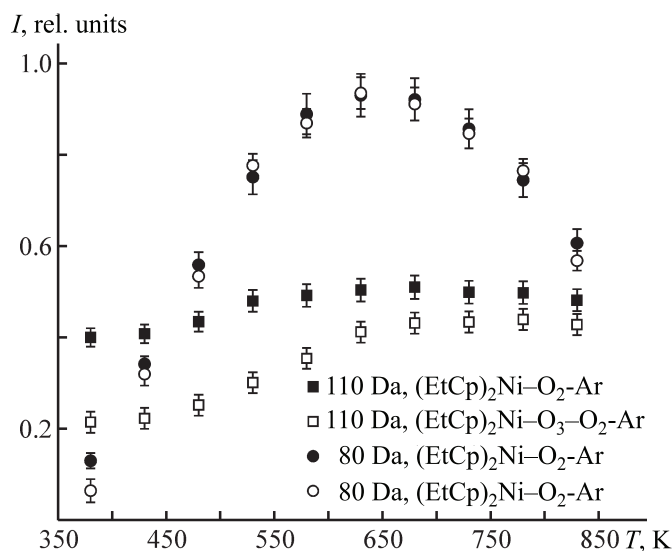

Fig. 5. Intensity I of ions with m/z 110 and 80 Da vs. temperature T in the absence and presence of ozone.

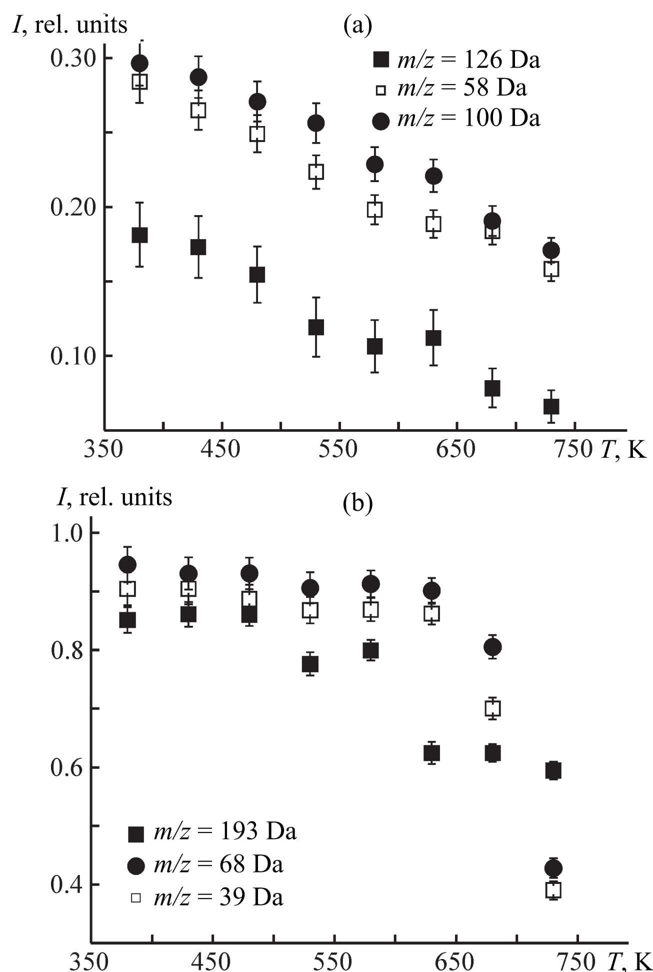

Fig. 6. Intensity I of the peaks with m/z (a) 126, 100, and 58 Da and (b) 193, 68, and 39 Da vs. temperature T.

The occurrence of reaction (5) is confirmed by the appearance of peaks corresponding to the substance with m/z 193 Da and its fragments (Fig. 6b) (m/z 39 and 68 Da) formed as a result of an electron impact, with the fragment ions corresponding to ions obtained in ionization of furan [19, 20],

The compound $C_8H_6O_2Ni$ was not observed in any of the conditions under study when the $(EtCp)_2Ni$–O–Ar system was examined. It is a nickel-containing compound additionally formed upon introduction of ozone. This circumstance suggests that the decrease in the growth rate of NiO layers, experimentally observed upon introduction of ozone, may be due to the consumption of the reagent for the $C_8H_6O_2Ni$ formation in the gas phase, which is in all probability not involved in the deposition of NiO layers.

The data furnished by atomic-force microscopy demonstrated that the surface of the layers has a grained structure, with the average grain diameter being about 90 nm. The results of an X-ray phase analysis indicate that there is a crystalline NiO phase with a cubic face-centered lattice with a parameter $a = 0.418$ nm in the layers. The average size of coherent scattering regions was 10 nm. The XPS data demonstrate that the composition of layers obtained in the $(EtCp)_2Ni$–O_3–O_2–Ar system shows a deviation from the stoichiometry toward the excess of oxygen, with Ni/O = 0.85 ± 0.02.

CONCLUSIONS

(1) A study of the fundamental physicochemical aspects of the chemical vapor deposition of NiO layers in the $(EtCp)_2Ni$–O_3–O_2–Ar system demonstrated that the deposition occurs under kinetic control in the temperature range 630–740 K and has an activation energy of 83 ± 5 kJ mol^{-1}. This temperatures is the working range for the technological process in reactors with “hot walls,” because the reagent is expended at higher temperatures for deposition of an oxide layer on the inner surfaces of the reaction chamber before the technological deposition zone and the process is limited by the delivery of the reagent into the reaction zone.

(2) It was shown that introduction of ozone as a stronger oxidizing agent does not make lower the lower limit of the deposition temperature range, but is accompanied by a decrease in the layer deposition rate,

compared with the deposition in the $(EtCp)_2Ni–O_2$-Ar system. The results of a mass-spectrometric analysis of the gas phase composition led to an assumption that the observed decrease in the growth rate of NiO layers may be due to the expenditure of the reagent for the formation of a by-product, $C_8H_6O_2Ni$, in the gas phase.

(3) The obtained evidence about the fundamental physicochemical aspects of the chemical vapor deposition of nickel oxide layers can serve as a basis for development of technological equipmment and industrial technology for deposition of NiO layers.

REFERENCES

1. Subramanian, B. and Ibrahim, M., *J. Mater. Sci. Mater. Electron*., 2009, vol. 20, pp. 953–957.
2. Melezhik, A.V., Romantsova, I.V., D'yachkova, T.P., et al., *Russ. J. Appl. Chem*., 2012, vol. 85, no. 5, pp. 782–787.
3. Nalage, S.R., Chougule, M.A., Sen, Sh., and Patil, V.B., *J. Mater. Sci. Mater. Electron*., 2013, vol. 24, pp. 368–375.
4. Lu, H.L., Scarel, G., Wiemer, C., et al*., J. Electrochem. Soc*., 2008, vol. 155, no. 10, pp. H807–H811.
5. Usha, K.S., Sivakumar, R., and Sanjeeviraja, C., *J. Appl. Phys*., 2013, vol. 114, no. 12, pp. 123501.
6. Nigro, R.L., Fisichella, G., Battiato, S., et al., *Mater. Chem. Phys*., 2015, vol. 162, pp. 461–468.
7. Nalage, S.R. Chougule, M.A., Sen, Sh., et al., *Thin Solid Films*, 2012, vol. 520, no. 15, pp. 4835–4840.
8. Guo, W., Hui, K.N., and Hui, K.S., *Mater. Lett*., 2013, vol. 92, pp. 291–295.
9. Jiang, D.Y., Qin, J.M., Wang, X., et al., *Vacuum,* 2012, vol. 86. no. 8, pp. 1083–1086.
10. Kada, T., Ishikawa, M., Machida, H., et al., *J. Cryst. Growth*, 2005, vol. 275, no. 1, pp. e1115–e1119.
11. Premkumar, P.A., Bahlawane, N., and Kohse-Höinghaus, K., *CVD*, 2007, vol. 13, pp. 219–226.
12. Wang, H., Zhao, Y., Li, X., et al., *Vacuum*, 2015, vol. 119, pp. 77–80.
13. Premkumar, P.A., Toeller, M., Adelmann, Ch., et al., *CVD*, 2012, vol. 18, pp. 61–69.
14. Yang, Y., Tao, Q., Srinivasan, G., et al*., ECS J. S. S. Sci. Tech*., 2014, vol. 3, no. 11, P345–P352.
15. An, W.J., Thimsen, E., and Biswas, P., *J. Phys. Chem. Lett*., 2009, vol. 1, no. 1, pp. 249–253.
16. Protopopova, V.S. and Alexandrov, S.E., *Russ. J. Appl. Chem*., 2012, vol. 85, no. 5, pp. 741–745.
17. Protopopova, V.S. and Alexandrov, S.E., *Surf. Coat. Techn*., 2013, vol. 230, pp. 316–321.
18. Jing Zhoua, Qian Zhaob, Wen-Wen Chenb, et al., *J. Am. Soc. Mass Spectrom*., 2010, vol. 21, no. 7, pp. 1265–1274.
19. Nie, S.P., Huang, J.G., Zhanget, Y., et al., *Food Control*, 2013, vol. 30, no. 1, pp. 62–68.
20. Dampc, M. and Zubek, M., *Int. J. Mass Spectrom*., 2008, vol. 277, no. 1, pp. 52–56.